Acta Materialia 103 (2016) 341–351

Contents lists available at ScienceDirect

Acta Materialia

journal homepage: www.elsevier.com/locate/actamat

Full length article

The effect of aluminium on twinning in binary alpha-titanium

Arnas Fitzner [a,b], D.G. Leo Prakash [a,c], Joao Quinta da Fonseca [a], Matthew Thomas [d], Shu-Yan Zhang [e], Joe Kelleher [e], Pascal Manuel [e], Michael Preuss [a,*]

[a] School of Materials, The University of Manchester, M13 9PL, UK
[b] Brunel Centre for Advanced Solidification Technology, Brunel University London, UB8 3PH, UK
[c] Materials Research Centre, College of Engineering, Swansea University, Bay Campus, Swansea SA1 8EN, UK
[d] Timet, PO Box 704, Witton, Birmingham B6 7UR, UK
[e] ISIS Facility, Harwell Oxford, Didcot OX11 0QX, UK

ARTICLE INFO

Article history:
Received 17 July 2015
Received in revised form 23 September 2015
Accepted 23 September 2015
Available online 6 November 2015

Keywords:
Deformation twinning
Ti–Al binary alloys
Neutron diffraction
EBSD
Short range ordering

ABSTRACT

The deformation mechanisms of binary Ti–Al model alloys (0–13.1 at.% Aluminium) have been investigated with respect to the twinning activity using in-situ loading in combination with neutron diffraction as well as detailed post mortem electron backscatter diffraction analysis. A consistent starting grain size and texture was generated for all alloys promoting tensile twinning during compression testing. Long-wavelength neutron diffraction and selected area diffraction transmission electron microscopy analysis were carried out to detect evidence of Aluminium ordering and Ti_3Al formation.

It was found that raising the Aluminium content in Titanium does first slightly enhance twinning, with $\{10\bar{1}2\}\langle 10\bar{1}1\rangle$ tensile twinning being by far the dominant type, while the critical residual intergranular strains for twin initiation decreases. This suggests that either the lowering of stacking fault energy by Aluminium or its solute solution strengthening effect are important factors. At around 7 at.% Aluminium a turning point in twinning activity was noticed and a further increase in Aluminium did result in a dramatic loss of twinning activity particularly when the material had been exposed to an additional low temperature age. The dramatic decrease of twinning activity is strongly correlated with increasing evidence of short range ordering and also early signs of Ti_3Al-formation in case of the highest Aluminium content. In addition, electron backscatter diffraction analysis revealed that the formation of Aluminium ordered zones do severely hinder growth of twin boundaries.

1. Introduction

Despite the importance of aluminium as an alloying element in commercial titanium alloys, its effect on deformation mechanism activity is still poorly understood. This is particularly true regarding its effect on twinning. In metals with a hexagonal close packed (hcp) crystal structure, twinning is often considered an important deformation mechanism as it offers shear with a <c> component. The only other mechanism that includes <c> component shear is pyramidal <c+a> slip, which is known to have a critical resolved shear stress (CRSS) about 3–4 times that of prismatic <a> slip in typical titanium alloys [1,2]. In principle, twinning improves formability and impact resistance because it increases work hardening rate during deformation [3]. Adding Al to Ti is known to reduce elongation to failure [4], cause unstable shear [1] and it has been argued that 6 wt.% Al (10 at.% Al) completely switches off twinning [2]. However, it is still unclear why Al affects twinning in Ti alloys.

Aluminium and oxygen are potent solid solution strengthening elements in α-Ti [5]. Aluminium is a substitutional element whereas oxygen is interstitial [2]. The effect of Al on the slip and twin activity has been studied in some detail in large single-crystal compression samples [1]. This work showed that the CRSS for basal and prismatic <a>-slip increases with increasing Al content. It was also shown that at 12 at.% Al, CRSS for basal <a> slip is slightly higher than prismatic <a> slip. In principle, this trend can be explained by Al decreasing the stacking fault energy on the basal plane [6,7], which is also known to have a significant effect on the high-temperature creep performance in α-Ti alloys [8,9]. The work of Williams et al. [1] also showed that CRSS for <c+a> slip is consistently more difficult than <a> slip.

* Corresponding author.
E-mail address: michael.preuss@manchester.ac.uk (M. Preuss).

http://dx.doi.org/10.1016/j.actamat.2015.09.048

Regarding twin activity and twin morphology, significant differences have been observed when comparing commercially pure (CP) Ti [10,11] and for instance Ti–6Al–4 V [12,13]. While in CP-Ti twin activity tends to be very high during the early stage of deformation and twins are readily observable, twin activity has often been reported to be less frequent, or even absent, in Ti–6Al–4 V [2]. The reason for this is not entirely clear but it has been suggested it is related to the smaller grain size, high Al content and the presence of Ti_3Al precipitates in Ti–6Al–4 V [2]. However, more recently, it has been shown that compression testing of Ti–6Al–4 V at room temperature leads to the development of a normal basal texture, which is generally associated with activation of $\{10\bar{1}2\}\langle 10\bar{1}1\rangle$ tensile twinning. Moreover, the same study suggests that despite the difficulty of twin nucleation in Ti–6Al–4 V, once twins have nucleated their growth is very rapid resulting in the consumption of entire parent grains, making the detection of twins by conventional means difficult [12].

For metals with an fcc crystal structure it has long been established that the propensity for twin nucleation is related to the stacking fault energy (SFE) as the stacking fault can act as a nucleation site for twin formation [14–16]. Interestingly, in the absence of ordering, Al does lower the SFE on the basal plane in Ti very substantially [9,17]. Although twins in Ti do not usually involve stacking faults on the basal plane, according to one of the models of heterogeneous twin nucleation, twins initiate and grow from stacking faults on twinning planes, forming zonal dislocations with a $\langle 10\bar{1}\bar{1}\rangle$ Burgers vector in the case of $\{10\bar{1}2\}\langle 10\bar{1}1\rangle$ tensile twins [18]. Although the effect of increasing Al content on this process cannot be easily estimated, its effect on basal SFE suggests it should make twin nucleation easier.

One way in which Al could affect twin activity is through solute solution strengthening [4,5], however it is not immediately clear whether this would promote or hinder twinning. On one hand, if solid solution strengthening affects the CRSS for slip but not for twinning, a higher flow stress should lead to higher twinning activity, simply because plastic deformation occurs at higher stress levels. However, adding Al not only strengthens the material but also changes the character of slip. This is a consequence of the tendency to create short range ordering (SRO) followed by long range ordering (LRO), i.e. Ti_3Al (α_2 – DO_{19} structure), depending on the level of Al addition and the heat treatment procedure. Studying ordering in Ti–Al alloy systems is notoriously difficult. A TEM study of Ti 15at.%Al (500 ppm O) after ageing for 80 h at 550 °C identified spherical α2 precipitates [19], which coarsened to ellipsoidal precipitates along the <c>-axis during continued ageing [19,20]. Signs of ordering have also been commonly reported at Al concentration as low as 8.5 at.% [2,4,21–23]. Namboodhiri et al. identified signs of SRO down to 7 at.% Al by resistivity measurements [24]. An adapted version of the phase diagram in Ref. [25] is presented in Fig. 1. Reported Ti_3Al domain sizes and ageing times are given for several concentrations and temperatures as marked in the phase diagram [1,4,20]. For comparison, the heat treatments used in the current study are also indicated.

These ordered domains or phases are expected to strengthen the material as shearing will either result in the formation of a diffuse anti-phase boundary (DAPB) in the case of SRO or the more familiar anti-phase boundary (APB) when LRO is fully developed [26]. First principle calculations suggest that the energy for the formation of a DAPB is about 4–8 times smaller than the APB energy for Ti_3Al. It has long been suggested that ordering promotes slip localisation [27] and more recent TEM investigations have indeed confirmed the formation of coupled dislocations in deformed Ti-6 wt.% Al [28]. The change in slip character to more localized slip with increased Al content could make the accommodation of the twinning strain in both the parent grain and the twinned volume more difficult, hindering twin growth. In aged material, the presence of Ti_3Al particles will also have an effect. Research on the TiAl–Ti_3Al system has consistently demonstrated that although TiAl forms deformation-twins, Ti_3Al does not [29–34], suggesting that ordering hinders twinning. In addition, some interesting recent studies of twin boundary mobility in a Mg–Gd alloy have also shown that ordering on twin boundaries exerts a very strong pinning force [35].

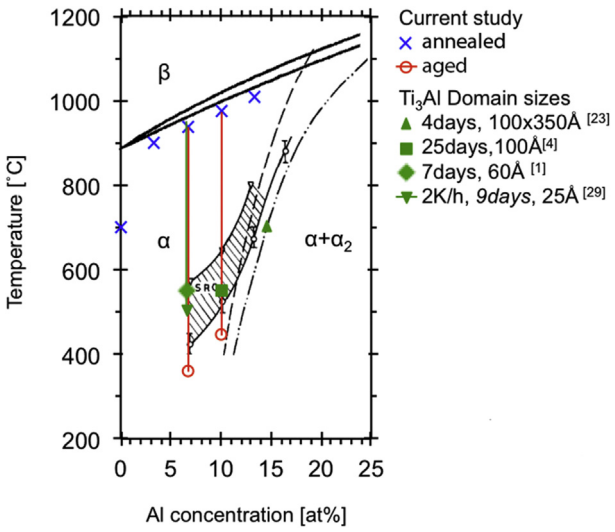

Fig. 1. Ti-rich side of the Ti–Al phase diagram adapted from Refs. [1,23,29,45,52] showing positions of annealing and ageing temperatures.

In summary, there is no convincing explanation for how adding Al to Ti affects twinning. Increasing the Al content increases the flow stress and decreases the SFE, all of which should promote twinning. On the other hand, it leads to slip localization and ordering, both of which should suppress twinning. In light of this lack of a clear understanding, and the absence of a systematic studies of the effect of Al on polycrystalline materials, a series of deformation studies were carried out on binary Ti–Al alloys with Al contents ranging from 0 to 13 at.%. To facilitate a meaningful comparison, great care was taken to generate starting microstructures with very similar recrystallized grain size and macroscopic texture. The microstructure was first characterised by SEM/EBSD, TEM and long-wavelength neutron diffraction to determine starting texture, grain size, lattice spacing and provide evidence of α_2 and SRO. In-situ neutron diffraction compression experiments were carried out to quantify twin activity and measure elastic strains along the c-axis in the grain family associated with the parent grains of twins. The methodology used is similar to previous work carried out on commercially pure Ti, Ti–6Al–4 V, Zr alloys and Mg alloys [36–41] to monitor the $\{10\bar{1}2\}\langle 10\bar{1}1\rangle$ tensile twin activity during compression testing. In the present work, the twin analysis was further complimented by detailed post-mortem EBSD analysis.

2. Materials and methods

2.1. Material preparation

For the purpose of this research, 200 g binary Ti–Al alloy buttons with different Al content up to 13 at.% Al (8 wt.% Al), were double melted in a tungsten arc furnace under an inert gas atmosphere. This was followed by β forging at 1100 °C at the TIMET research facility in Witton, UK. Subsequently, the buttons were cross-rolled into a bar (14 × 14 × 260 mm) on a “2 high Robertson mill”

(WHA Robertson & Co Ltd) at 750 °C in the case of the high purity Ti button (from here on called Ti–0Al) and at 870 °C when containing Al. Ti–0Al was recrystallised (RX) at 750 °C, 130 °C below the β transus temperature, in a tube furnace under an argon shield for 5 h followed by air-cooling, while recrystallisation treatments for the Al containing bars were carried out 30 °C below the β-transus, followed again by air cooling. The β-transus depends on Al content and therefore, Ti–3Al, Ti–7Al, Ti–10Al and Ti–13Al (all at.%) were recrystallized at 895 °C, 933 °C, 968 °C and 990 °C, respectively. The β-transus temperatures were determined using Thermocalc, which is known to provide reasonably accurate results for this range of alloys [25,42,43]. Ti–0Al was annealed at a lower temperature relative to the β-transus than the binary alloys in order to achieve a similar final grain size. In addition, some Ti–7Al and Ti–10Al samples were cooled at 10 °C/h from RX temperature to 380 °C and 420 °C respectively, around 30 °C below the α_2-solvus temperature [25], and aged for 120 h to promote α_2 formation. The different heat treatment procedures are listed in Table 1. Chemical analyses were performed after annealing by TIMET, Savoie, France using inductively coupled plasma mass spectrometry on a HORIBA Ultima2 for the analysis of metallic elements, on a HORIBA EIMA 820 V for carbon analysis and on a LECO EF-400 for oxygen and nitrogen analysis. Table 2 lists the measured chemical composition of the binary alloys displaying oxygen (O) concentration of 1000 ± 500 ppm, while carbon and nitrogen are below 100 ppm. Rectangular and cylindrical samples of $6 \times 6 \times 9$ mm^3 and 6 mm diameter and 9 mm length were machined for ex-situ compression testing while for in-situ loading, using neutron diffraction, cylindrical samples of 8 mm diameter and 12 mm length were required.

2.2. Microstructure analysis

Cross sections with the plane normal parallel to the rolling direction (RD) were cut from the middle of non-deformed and deformed samples and prepared by standard mechanical grinding followed by oxide particle suspension (OPS) polishing with intermediate Kroll's etching for 10 s (3% hydrofluoric acid, 6% nitric acid and balance water) to produce mirror finish for optical microscopy (OM), x-ray diffraction (XRD) and electron backscattered diffraction (EBSD). The texture was measured using EBSD on a CamScan Maxim 2500FEG SEM operated at 20 kV and equipped with a NordLYS detector. Measurements were carried out using a 40 μm step size on areas of at least 4×4 mm^2, covering more than 3500 grains. The macrotexture measurements were used to approximate the $\{10\,\bar{1}2\}\langle 10\,\bar{1}1\rangle$ twin activity A_{twin} based on texture changes by using Equation (1), where N_{RX} is all indexed EBSD data points before deformation, n_{RX} is a subset within 30° to the loading direction (LD), N_s is all EBSD data points of the deformed sample and n_s is a subset within 30° to LD.

$$A_{twin} = n_S/N_s - n_{RX}/N_{RX} \quad (1)$$

Table 1
Heat treatment and grain size.

Alloy	α-solution anneal		Ageing		Mean grain size [μm]
	T [°C]	t [h]	T [°C]	t [h]	
Ti–0Al	750	5	–	–	94
Ti–3Al	895	5	–	–	82
Ti–7Al	933	5	–	–	73
Ti–7Al-aged	933	5	380	120	74
Ti–10Al	968	5	–	–	71
Ti–10Al-aged	968	5	420	120	77
Ti–13Al	990	5	–	–	78

It should be pointed out that any great degree of reorientation of the hexagonal close packed (hcp) crystal at small strain levels is unlikely to be related to slip, as slip creates a more gradual texture change [44]. It should also be noted that 65° compression twins ($\{11\,\bar{2}2\}\langle \bar{1}123\rangle$) would decrease A_{twin}, while 35° tensile twins ($\{11\,\bar{2}1\}\langle \bar{1}126\rangle$) could increase it [44].

Detailed orientation maps were recorded on a FEI Sirion FEG SEM using a step size of 1 μm and recording maps covering typically 100 grains or more. Data were cleaned and analysed using the commercial software package HKL. Twin boundary criteria, as given by Bozzolo et al. [45], were used to identify and quantify relative area fractions of twin systems.

Thin foils for transmission electron microscopy (TEM) were prepared for selected conditions by electro polishing (6% perchloric acid (60%) and 94% methanol) between –50 and –35 °C at 15 V using a Tenupol 5. A FEI Tecnai T20 equipped with a LaB6 filament was used at 200 kV and selected aperture electron diffraction images were taken using Ditabis image plates that provide a high dynamic range enabling the detection of faint Ti_3Al superlattice reflections.

Long-wavelength powder diffraction type measurements were carried out at the time-of-flight (ToF) beam line WISH, based at the ISIS neutron spallation facility, UK, to assess the state of ordering (SRO, LRO) [46]. Cylindrical bulk samples of 8 mm diameter and 40 mm length were loaded in one of two Vanadium cans of 150 μm wall thickness and mounted on an Al candlestick. Boron nitride shielding was used to avoid scattering from the Al holder. The samples were aligned in the centre of the beam gauge volume (20×40 mm) and 60 min long measurements were taken at pressures below 0.05 bar. Background subtracted spectra from bank 3 (at 90° from the incident beam), which provided the highest flux for the d-spacing region of interest, were smoothed with averaging over 20 points.

2.3. Mechanical testing

Standard room temperature compression tests were conducted on an Instron 5569 at an initial strain rate of 10^{-3} 1/s. The use of Lubriplate grease minimized barrelling of the sample and helped ensure an uniaxial stress state during deformation. Samples for microstructural and texture observation were strained monotonically to plastic strains of ε_{pl} = 1.7%, 3.7% and 8.7% along the rolling direction (RD).

2.4. In-situ loading using neutron diffraction

In-situ compression experiments using neutron diffraction were carried out at the ENGIN-X beam line, which is also based at the neutron spallation facility ISIS, UK. ENGIN-X is also a ToF instrument with two detectors installed at 90° to the incoming beam [47,48]. With a loading rig (an Instron 8562 with 100 kN load cell) positioned at a 45° angle to the incident neutron beam, as shown schematically in Fig. 2, the two detectors allow recording of diffraction spectra parallel (red areas) and transverse (blue areas) to the loading direction (LD). The samples were incrementally loaded but the measurements were carried out in the unloaded condition to avoid significant cold creep during neutron diffraction measurements. For each loading experiment about 14 diffraction measurements were carried out within the plastic regime up to 9% plastic strain. A current of 30 μA was collected for each data point to ensure a good signal-noise ratio, which took 24 min under optimal beam conditions.

The axial detector was used to monitor twinning. Since the most common twinning mode in Ti alloys is the $\{10\,\bar{1}2\}\langle 10\,\bar{1}1\rangle$ tensile twin, which provides a near 90° rotation of the c-axis from a tensile

Table 2
Measured chemical composition and lattice parameters of model alloys.

Alloy	Al [wt.%]	Al [at.%]	C [ppm]	N [ppm]	O [ppm]	Ti	*a* [Å]	*c* [Å]
Ti–0Al	0.00	0.0	55	13	507	bal.	2.949	4.683
Ti–3Al	2.00	3.49	72	39	474	bal.	2.942	4.681
Ti–7Al	3.90	6.67	50	23	413	bal.	2.935	4.678
Ti–7Al-aged	3.90	6.80	50	23	592	bal.	2.935	4.677
Ti–10Al	5.88	10.01	76	53	756	bal.	2.929	4.675
Ti–10Al-aged	5.88	9.99	76	53	567	bal.	2.928	4.673
Ti–13Al	7.85	13.13	55	94	377	bal.	2.925	4.669

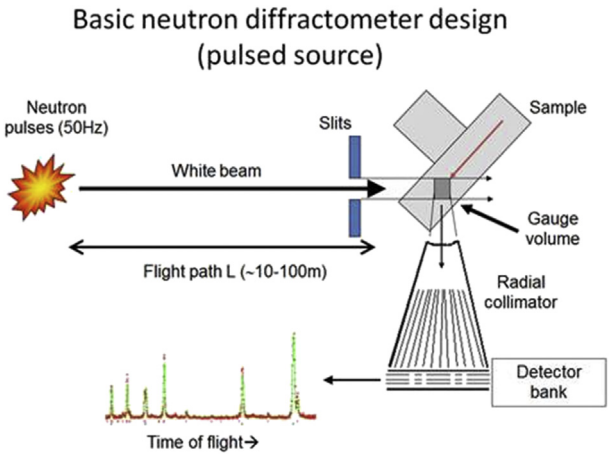

Fig. 2. Shematic of experimental setup at ENGIN-X, ISIS for in-situ loading experiment with detector areas axially in red and transverse in blue and {0002}-pole figure before (left) and after loading (right). (For interpretation of the references to colour in this figure legend, the reader is referred to the web version of this article.)

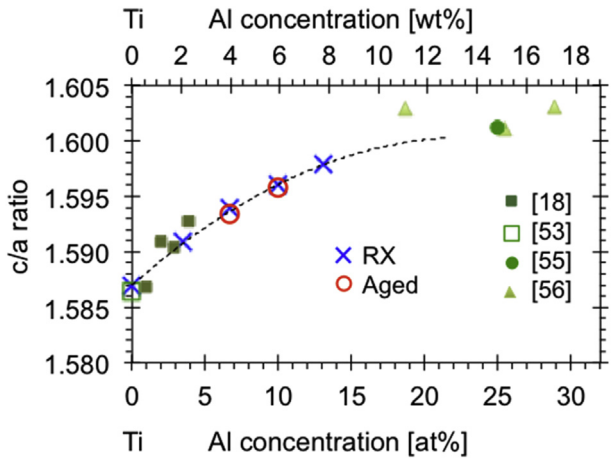

Fig. 3. Calculated c/a ratio as function of the aluminium concentration in comparison to literature values.

to a compressive stress condition, twinning causes an increase in the 0002 peak intensity along the loading direction during compression loading. In addition the transverse detector was used to monitor the (residual) elastic strain of the grains that are most likely to twin by measuring shifts in the position of the 0002 reflection. Single peaks were fitted using the in-house ISIS software Open Genie. The lattice strain evolution was calculated as described by Warwick et al. [38]. In addition, the diffraction elastic constant (DEC) recorded for the 0002 reflection of the individual alloys was used to calculate the 0002 intergranular strains in the loaded condition.

The initial lattice spacing of each alloy was determined by Rietveld analysis of the spectra recorded on each detector before loading and averaging the results.

3. Results

3.1. Starting material

Neutron diffraction results presented in Table 2 show that the *a* lattice parameter decreases comparatively linearly with increasing Al content while the *c* lattice parameter decreases more rapidly at high Al concentrations. The corresponding *c*/*a* ratios are plotted in Fig. 3, and are in excellent agreement with previously reported values [49,50]. The data show a clear non-linear relationship between Al concentration and c/a ratio, which indicates that with increasing Al content some of it is not kept in solution. Interestingly, when extrapolating the nonlinear trend to higher Al levels, the c/a ratio approaches the values in the literature for Ti_3Al [51,52].

Fig. 4a and b displays the diffraction profiles recorded on WISH focussing on the large d-spacing range in order to identify a possible $\{11\bar{2}0\}$ α_2 superlattice reflection. The profiles are presented separately in terms of effect of Al addition (Ti–0Al, Ti–7Al, Ti–10Al and T–13Al), Fig. 4a, and comparing between annealed and aged conditions, Fig. 4b. None of the patterns showed any evidence of distinct α_2 superlattice reflections. However, a broad intensity increase becomes noticeable in the region where one would expect the $\{11\bar{2}0\}$ and $\{10\bar{1}1\}$ α_2 reflection in the case of Ti–10Al and Ti–13Al, Fig. 4a. Ageing of Ti–7Al also causes a small intensity increase in this range while ageing Ti–10Al makes this shoulder even more pronounced, Fig. 4b.

Extensive TEM analysis was carried out in order to detect α_2 superlattice reflections in the binary alloys with relatively high Al content. Selective area electron diffraction pattern analyses with the zone axis along $[10\bar{1}0]$ showed no indication of an α_2 superlattice reflection in Ti–10Al, Fig. 5a, while the aged Ti–10Al displayed a very weak superlattice reflection spot, Fig. 5b. In both cases very significant scattering was seen in the region of the expected superlattice reflection, which impaired the clear visualisation of the superlattice spot in the aged Ti–10Al.

EBSD was used to map the starting microstructure and at strains of 0.02, 0.04 and 0.09 (ex-situ). The first row of Fig. 6 (small crop from significantly larger EBSD maps) shows representative inverse pole figure (IPF) colour orientation maps of the starting microstructures, with the corresponding 0002 and $10\bar{1}0$ pole figures (obtained from larger areas) shown in Fig. 7a. While the grain size distribution appears to be somewhat heterogeneous for all alloys, no significant differences were noticeable between alloys, including with respect to macrotexture. Large EBSD maps did not reveal any regions of strong microtexture (macrozones). The mean grain size in all alloys was about 80 μm with very low misorientations (<2°) within grains. All starting microstructures displayed a very low mud (multiples of uniform density) value along RD in the 0002 pole figure, Fig. 7a. The distribution of the basal poles within the clockwork texture is rather random in Ti–0Al and Ti–3Al and Ti–13Al, while Ti–7Al and

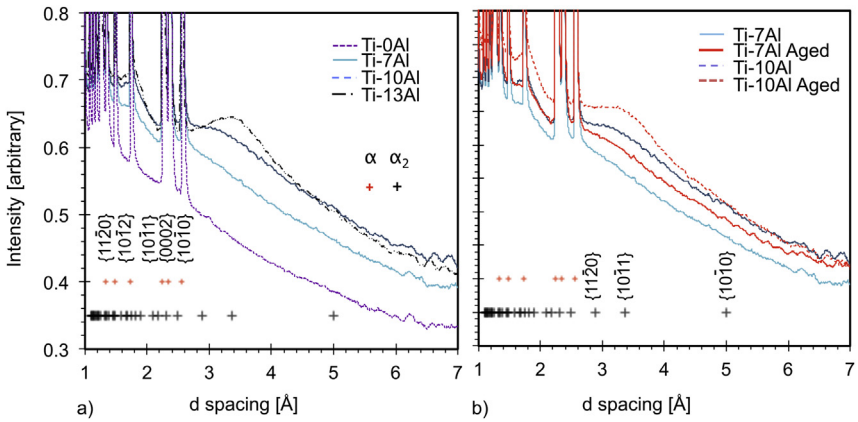

Fig. 4. Long-wavelength diffraction spectra showing a) effect of Al concentration and b) effect of ageing.

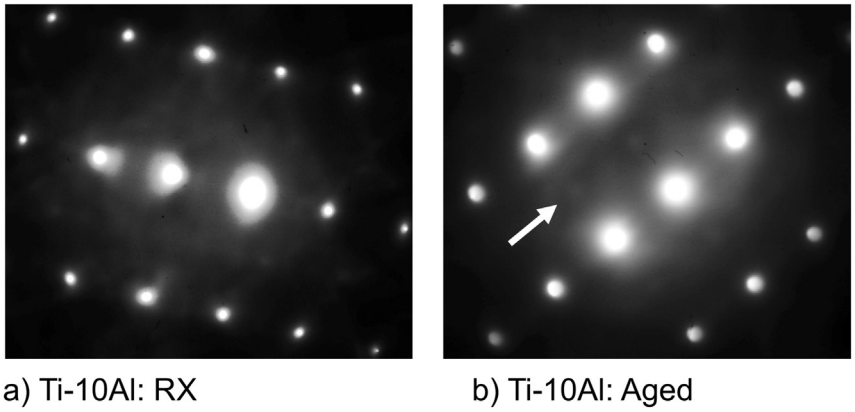

Fig. 5. Selected area electron diffraction pattern images recorded on the $(10\bar{1}0)$ zone axis using a camera length of a) Ti–10Al in annealed condition and b) after ageing. Note the faint diffuse α_2 reflections marked by the white arrow.

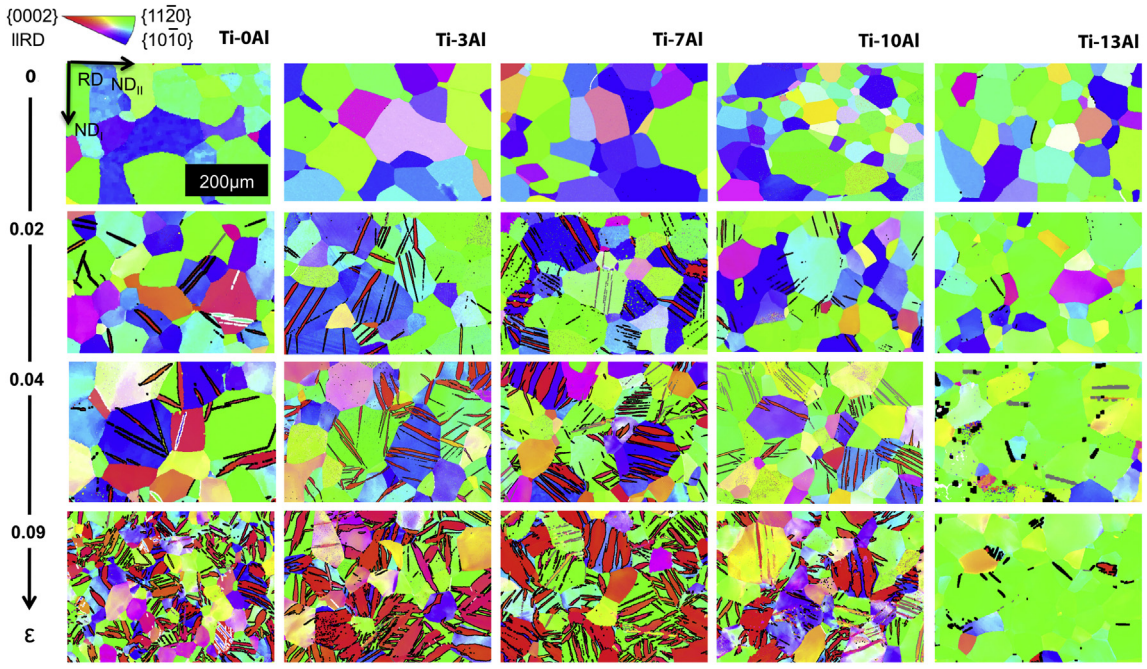

Fig. 6. Orientation maps in IPF colouring//LD//RD of the starting conditions (Ti–0Al–Ti–13Al) and at compressive strains of 0.02, 0.04 and 0.09. Please note that these are ex-situ measurements, i.e. different samples for each strain value. Twin boundaries are indicated as: Black = {10 $\bar{1}$ 2}<10 $\bar{1}$ 1>, Grey = {11 $\bar{2}$ 1}< $\bar{1}$126>, White = {11 $\bar{2}$ 2}< $\bar{1}$123>.

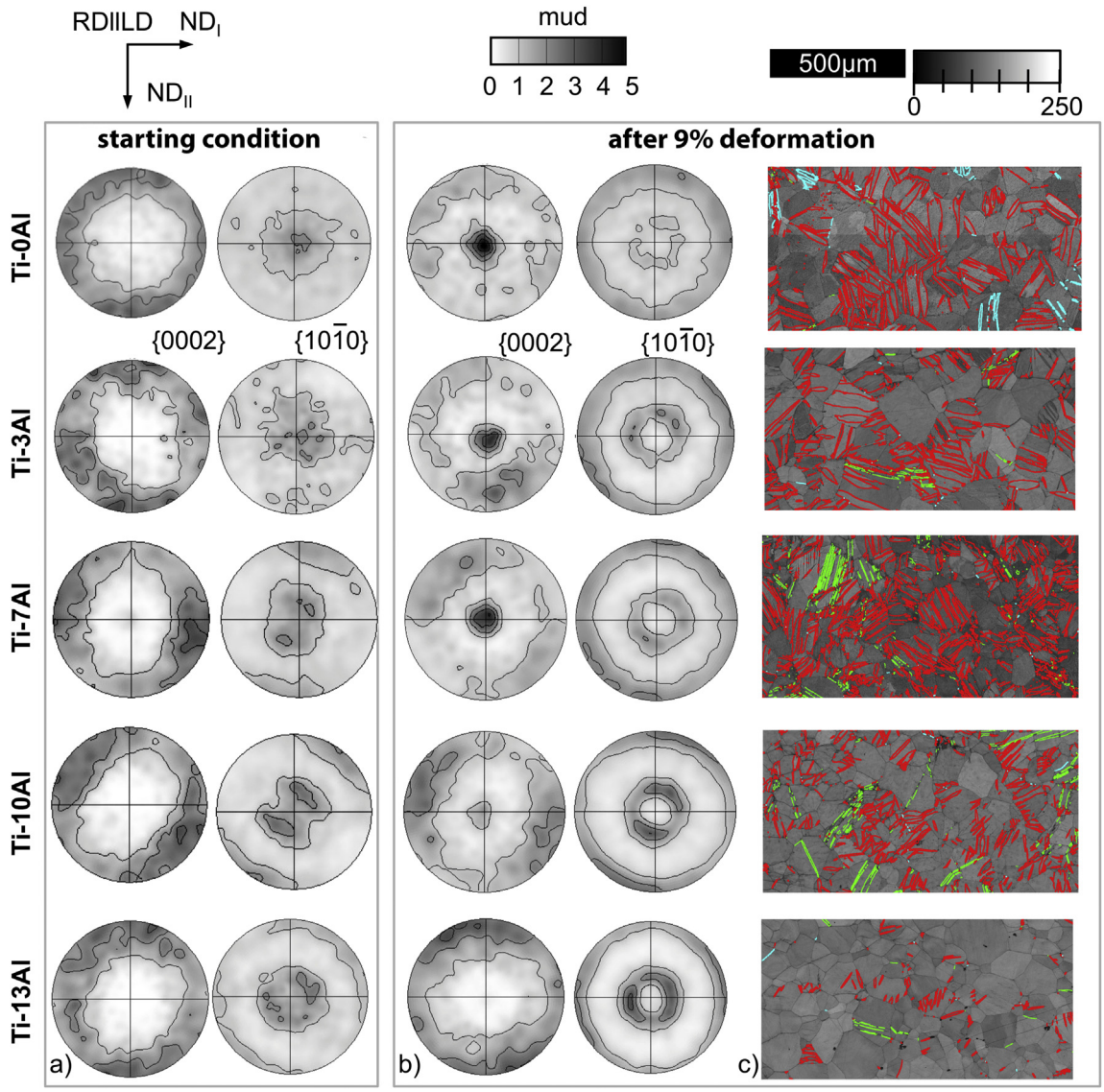

Fig. 7. a) Pole figure maps of the starting microstructure and b) after approximately 9% compression parallel to RD. In addition, c) displays close up band contrast maps highlighting twin types by different boundary colours: Red = {10 $\bar{1}$ 2}<10 $\bar{1}$ 1>, Green = {11 $\bar{2}$ 1}< $\bar{1}\bar{1}$26>, Blue = {11 $\bar{2}$ 2}< $\bar{1}\bar{1}$23>. (For interpretation of the references to colour in this figure legend, the reader is referred to the web version of this article.)

Ti–10Al display intensity maxima 45° between both ND directions. In Ti–0Al and Ti–3Al the $10\bar{1}0$ pole figures show a slight alignment along RD, while in the other alloys the $10\bar{1}0$ poles along RD are more split.

3.2. Flow curves

The flow curves for uniaxial compression along the rolling direction (RD) are presented in Fig. 8a). The mechanical response during the interrupted in-situ loading experiment using neutron diffraction reflects the behaviour of monotonic compression tests well, as indicated by the crosses for Ti–13Al. As one would expect, the yield strength increases significantly with Al content. It is noticeable that the increase in strength is most significant until 10 at.% Al, but far less pronounced with a further increase to 13 at.% Al. Ageing does not increase the 0.2% yield strength but causes a noticeable drop in work hardening rate. Fig. 8b) plots the work hardening rate as a function of compression strain. It can be seen that the ability to work harden increases with Al content but reaches a maximum for Ti–7Al. Higher Al contents give lower work hardening ability, as does ageing with the aged Ti–10Al material displaying the minimal work hardening rate θ_{min} during the early stage of plasticity.

3.3. Deformation microstructures and textures

As described earlier, the texture development during uniaxial compression testing gives a good indication of the development of {10 $\bar{1}$ 2}<10 $\bar{1}$1> tensile twinning. Any rotation caused by tensile twinning will result in the *c*-axis "rotating" towards the loading direction (LD), and a corresponding increase in intensity in the basal pole figures. Fig. 7b shows the 0002 and 10 $\bar{1}$0 pole figures after true strain compression of about 0.09. It can be clearly seen that a strong basal pole does indeed develop along LD for Ti–0Al, Ti–3Al and T–7Al. In contrast, the 0002 pole figure of Ti–10Al only exhibits a very weak pole parallel to LD while for Ti–13Al the pole figure appears relatively unchanged compared to the starting condition.

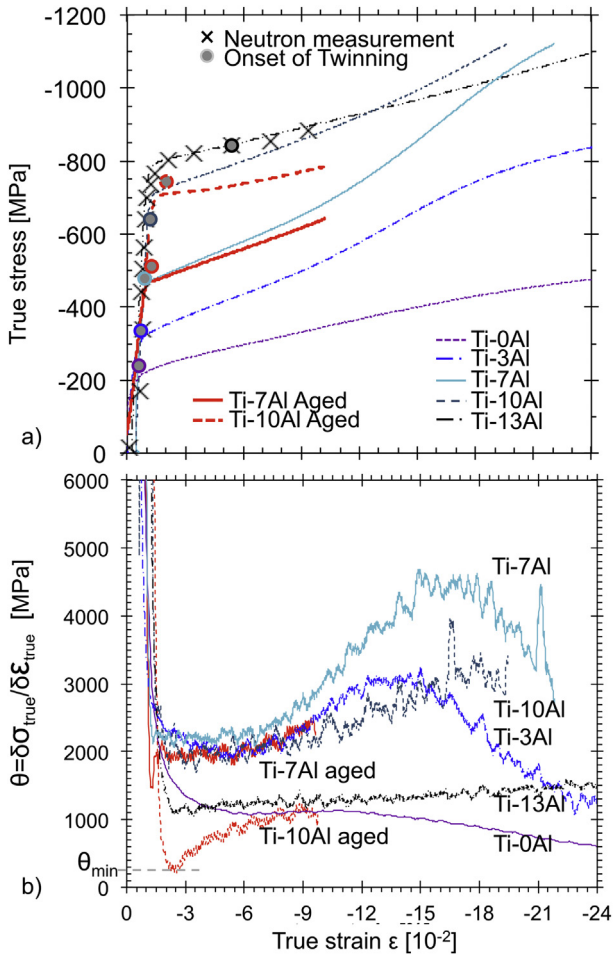

Fig. 8. a) True stress–strain curves recorded during quasi-static compression along RD. In the case of Ti–13Al data points from the in-situ loading experiment using neutron diffraction has been added to demonstrate similarity. b) Work hardening rate θ as function of the true strain.

These differences in texture evolution are consistent with observation from the orientation maps. Fig. 6 displays representative IPF colour orientation maps after about 0.02, 0.04 and 0.09 true strain. It is noticeable that for Ti–Al binary alloys with up to 7 at.% Aluminium several twins have formed within individual grains during the early stage of plastic deformation, which seem to grow in width during further straining to 0.09. This trend becomes more pronounced with increasing Al content, eventually showing large fractions of grains being consumed by twins, particularly for Ti–7Al. A further increase of Al concentration reduces the twinning activity Taking the example of Ti–13Al, there is still a significant number of twins that form but they have only just started to grow from one side of the grain boundary and have not grown in width. Accordingly, the data recorded for Ti–10Al and Ti–13Al, particularly after very small levels of plastic deformation, suggest that twins have predominantly nucleated from grain boundaries. Fig. 6 also illustrates that most grains that twin have one of their {10 $\bar{1}$0} normal nearly parallel to the loading direction (blue parent grains). Fig. 7c confirms the dominance of {10 $\bar{1}$2}<10 $\bar{1}$1> tensile twinning. Overall, the EBSD analysis suggests an increasing fraction of {10 $\bar{1}$2}<10 $\bar{1}$1> twins until 7 at.%Al, which drops dramatically with further Al addition. Only in the case of Ti–0Al about 4% {11 $\bar{2}$2}<$\bar{1}\bar{1}$23> were compression twins observed. The analysis also revealed that there is a very small fraction of {11 $\bar{2}$1}<$\bar{1}\bar{1}$26> tensile twins, which increases slightly with Al concentration, especially from Ti–3Al to Ti–7Al and again peaks for Ti–7Al.

The maximum accommodated strain from twinning can be approximated by using Equation (2), where s is the twin shear for a specific twinning systems and the corresponding twinning volume fraction V_{Twin}, [52].

$$\varepsilon_{max_i} = \sum\left(\sqrt{1/2}sV_{Twin}\right)_i \tag{2}$$

$$\varepsilon_{max} = \sqrt{1/2}0.176\cdot V_{TT1} + \sqrt{1/2}0.630\cdot V_{TT2} + \sqrt{1/2}0.217\cdot V_{CT} \tag{3}$$

Assuming that the measured area fractions by EBSD equal the volume fraction V_{Twin}, and considering the shear values associated with the three identified twin systems, the total twin strain ε_{max} was calculated for each alloy. This analysis revealed that after 0.09 true strain, 50–60% of the total strain had been accommodated by twinning in the case of Ti–0Al, Ti–4Al and Ti–7Al while this number dropped very rapidly to values of around 30% and 15% for Ti–10Al and Ti–13Al respectively.

3.4. Diffraction peak evolution

The starting texture of the different alloys and the choice of loading direction (RD) meant that the initial 0002 diffraction peak measured along the loading direction (axial detector) was too weak to be fitted satisfactorily. Once twinning initiated, a sufficiently strong 0002 reflection was measured along LD and the change in 0002 integrated intensity is given as a function of true strain in Fig. 9. The slope in Fig. 9 is an indication of the twinning activity. Fig. 9a shows the effect of Al content on twinning activity while Fig. 9b illustrates the effect of ageing for Ti–7Al and Ti–10Al. The slopes for Ti–0Al, Ti–3Al and Ti–7Al are essentially identical in Fig. 9a, indicating similar twinning activities. However, when the Al content is further increased, the twinning activity is substantially reduced with almost no sign of twinning for Ti–13Al. In addition, the critical true strain for twinning increases to more than 0.04 for Ti–13Al compared to around 0.01 for the other alloys. Fig. 9b demonstrates that ageing Ti–7Al has only a minor effect on twinning activity, while ageing Ti–10Al causes a more significant drop in twinning activity.

The 0002 diffraction peak along the transverse direction includes the grains ideally orientated for tensile twinning. Because of the starting texture, these grains make up the majority of the grains in this family. As the measurements were carried out in the unloaded condition, the peaks shifts are a measure of the residual lattice strains in the 0002 grain family. As it can be seen in Fig. 10, these grains are in residual tension after unloading. This residual strain increases until twinning starts, which can be inferred from the intensity plots in Fig. 9. During further deformation and unloading, the residual lattice strain decreases steadily. As with Figs. 9 and 10 is split into comparing the effect of Al (Fig. 10a) and the effect of ageing treatment (Fig. 10b). The maximum residual lattice strain in this grain family first decreases with Al content before increasing dramatically for Ti–10Al and Ti–13Al. With the exception of Ti–13Al, the onset of twinning represents a sharp turning point regarding the residual lattice strain evolution. Ageing increases the critical residual lattice strain at twin initiation significantly for both Ti–7Al and Ti–10Al.

3.5. Summary of results

A summary of the results obtained from Ti and Ti–Al binary alloys is presented in Fig. 11. It demonstrates that the greatest gain in 0.2% yield strength was achieved between Ti–3Al and Ti–10Al while the

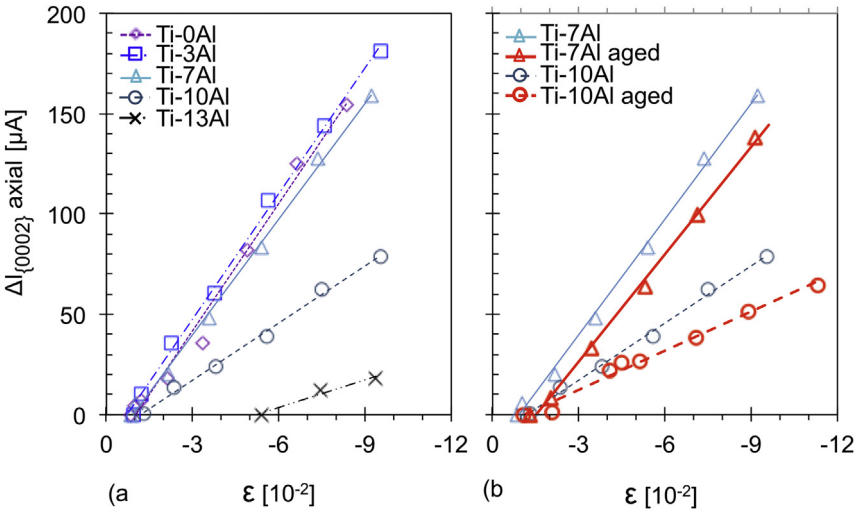

Fig. 9. Change of 0002 integrated intensity measured in the loading direction versus true strain highlighting a) effect of Al additions and b) the effect of ageing.

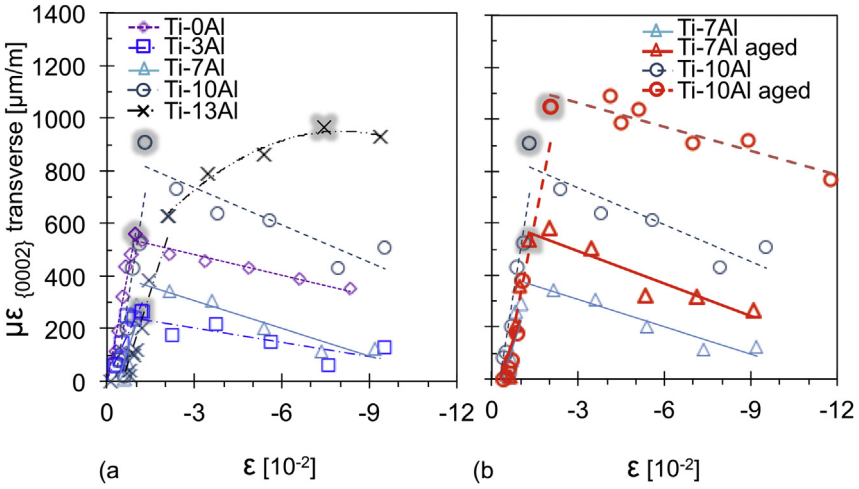

Fig. 10. Evolution of transverse lattice strain on {0002}-plane $\mu\varepsilon_{\{0002\}}$ as function of true strain highlighting a) effect of Al additions and b) the effect of ageing. The onset point of twinning is marked in grey.

ageing procedure applied for Ti–7Al and Ti–10Al had no noticeable effect on strength, Fig. 11a. The minimum work hardening rate θ_{min}, which for uniaxial compression along RD is in principle obtained before the onset of twinning, showed a slight maximum for Ti–7Al. Here, ageing resulted in a very significant drop of θ_{min} particularly in the case of Ti–10Al, Fig. 11b. The approximated $\{10\,\bar{1}2\}\langle 10\,\bar{1}1\rangle$ twin fraction suggests an increase of twinning activity with increasing Al content up to Ti–7Al but a sharp fall after that resulting in almost no twinning for Ti–13Al. Ageing of T–7Al and Ti–10Al further reduces twinning, Fig. 11c. Analysis of detailed orientation maps revealed some $\{11\,\bar{2}2\}\langle \bar{1}\bar{1}23\rangle$ compression twins only in the case of the high purity Ti sample and a small volume fraction of $\{11\,\bar{2}1\}\langle \bar{1}\bar{1}26\rangle$ tensile twins increasing with Al content and seemingly independent of the final heat treatment condition, Fig. 11d. Overall, similar trends were seen when monitoring the evolution of the change of (0002) integrated intensity during the in-situ loading experiments using neutron diffraction. In Fig. 11e the $\{10\,\bar{1}2\}\langle 10\,\bar{1}1\rangle$ tensile twin activity is represented by a simple linear regression of $\delta\Delta I_{(0002)}/\delta\,\varepsilon$ for each alloy composition. Although the increasing twinning activity from Ti–0Al to Ti–3Al or even Ti–7AL is not obvious, the drop after that is dramatic. The corresponding macroscopic stress values for twin initiation are plotted in Fig. 11f demonstrating a significant increase in macroscopic stress level with Al addition. The intercept of that slope with $\Delta I_{(0002)} = 0$ indicates the critical plastic strain for the onset of twinning as shown in Fig. 11g. It can be seen that the critical plastic strain decreases initially until 7 at.% Al. For Ti–13Al a sharp increase is noted.

Finally, Fig. 11h summarises the critical twin nucleation residual lattice strain $\varepsilon\mu_{\{0002\}}$ along the c-axis in the grain family that includes the grains most likely to twin. This value seems to be lowest for Ti–3Al but increases significantly beyond Ti–7Al. Ageing Ti–7Al or Ti–10Al slightly increases the critical lattice strain value.

4. Discussion

The initial slight increase in twinning activity followed by the dramatic drop implies that adding Al to Ti promotes twinning at lower Al contents and hinders it after a critical Al content is reached. In order to elucidate this observation, the different microstructural and plasticity aspects are critically discussed in terms of their possible contribution to twinning activity.

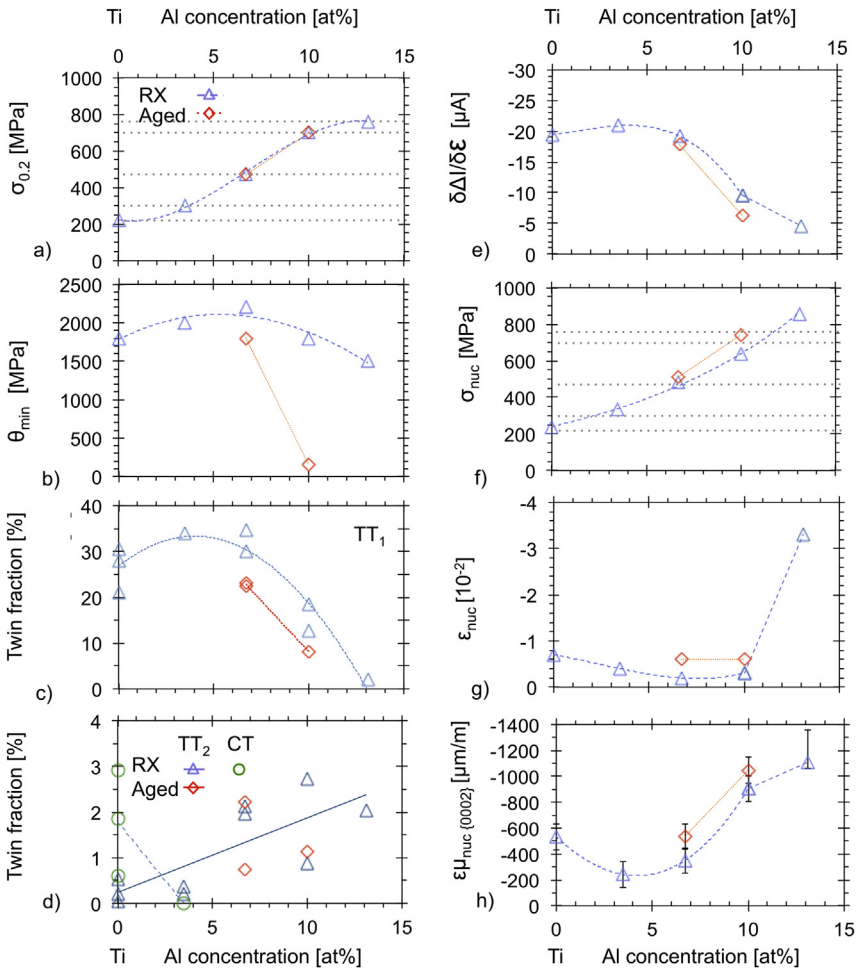

Fig. 11. Summary of the results for high purity Ti and the different Ti–Al binary alloys showing a) 0.2% proof strength $\sigma_{0.2}$; b) minimal work hardening rate θ_{min}; c) fractions of $\{10\bar{1}2\}10\bar{1}1$-twin; d) fractions of $\{11\bar{2}1\}\bar{1}126$ twins and $\{10\bar{1}1\}10\bar{1}2$ twins; e) twin activity $\delta\Delta I(0002)/\delta\varepsilon$; f) true stress to initiate twinning; g) critical plastic strain for onset of $\{10\bar{1}2\}10\bar{1}1$ twinning; h) residual 0002 lattice strain in the transverse direction.

4.1. Ordering in Ti–Al binary alloy

Several of the experimental results provide evidence of ordering starting with Ti–10Al. In the case of Ti–7Al, the aged condition seems to show a very slight indication of ordering in the long-range diffraction pattern. However, the long-wavelength neutron diffraction data provide no clear evidence of α_2 superlattice reflections but rather a broad increase in intensity. The detailed TEM analysis only revealed very weak α_2 reflections once Ti–10Al had been aged. Hence, both characterisation studies combined might suggest that once the Al content reaches 7 at.% SRO develops during ageing, which clearly becomes very dominant with increasing Al content and ageing. From about Ti–10Al aged, in addition to SRO, a small degree of LRO seems to be present. It is particularly interesting to note that the start of LRO does not result in a reduction of SRO. These observations are further supported by a more indirect observation in Fig. 2 showing a non-linear relationship between c/a ratio and Al concentration. Such deviation from linearity has been previously attributed to increased levels of ordering in other systems, for example in Ref. [53] where it was attributed to Cu_3Au formation in the Cu–Au system. The present observations are also consistent with results from Nambodhiri's resistivity measurements, showing effects of SRO down to 6.8 at.% Al [24], as indicated in Fig. 1.

It might be surprising that Ti–10Al and particularly Ti–13Al did not form α_2 more readily. However, the reader is reminded here that cooling rates from recrystallisation temperatures were in the range of 100 K/min (air cool of 14×14 mm^2 cross sectional samples) and ageing temperatures were substantially lower (see Table 1) than in cases when α_2 has been observed previously. For instance, α_2 in primary α of Ti–6Al–4 V is normally induced by ageing at 500 °C [2].

Regarding the effect of SRO on deformation mechanisms and twinning, the dramatic increase of 0.2% yield strength between Ti–3Al and Ti–10Al demonstrates that SRO does have a strong strengthening effect. However, it also clearly reduces work hardening rates and promotes planar slip as pointed out previously in Ref. [26].

4.2. Twinning in Ti–Al binary alloys

When studying the effect of alloying elements on twin activity it is important to ensure that the starting texture and grain sizes are similar for all compositions, as both aspects will affect twinning activity to some extent. In this work, a common starting texture was achieved via careful thermomechanical processing, which has a strong preferred alignment of the c-axis perpendicular to the

compressive loading direction and high Schmid factors for prismatic slip and tensile twinning.

The mechanisms of twin nucleation and growth in metals with an hcp crystal structure are still not well understood. The heterogeneous twin nucleation and growth have been discussed in terms of formation of zonal twinning dislocations and stress concentrations at grain boundaries [18]. These considerations ignore the need for the local twin shear to be accommodated so that any back stresses inhibiting twin growth are relaxed. This means that ease of deformation by slip in the parent grain will also impact twin activity. On the other hand, since in Ti, like in Zr, twinning is preceded by slip, an increase of the yield strength also means that twinning occurs at higher stresses.

Combining information from neutron diffraction and EBSD suggests that the initial slight increase of twinning activity with increasing Al content is related to easier growth rather than more nucleation. It is not clear at the moment if this observation is driven by a decrease in SFE [6,7,9,17,54], which in principle affects dissociation of basal rather than prismatic dislocations or if growth is driven simply by higher stresses at which plasticity starts and misfit strains are generated. It is however noticeable that the residual lattice strain for twin nucleation does initially decrease giving indication that twin formation becomes easier before ordering is observed.

Once ordering is observed, there is a clear reduction in twinning activity and with increasing evidence of ordering, this trend becomes more pronounced resulting in almost a complete suppression of twinning for Ti–13Al. Interestingly, ordering in the present case might mean mainly SRO. Calculations of the anti phase boundary (APB) energy created by a single basal or prismatic dislocation shearing SRO (diffuse) in the Ti–Al system gave a value of 25 mJ/m^2, which compares with 100–250 mJ/m^2 when shearing α_2. Those calculations suggest that any diffuse APB energy required for twinning a SRO cluster is comparatively small. However, it is worth remembering that Ti_3Al as an alloy does not twin [29–34] and the EBSD maps of the deformed samples show very clearly that once ordering is observed, twin growth declines very sharply. In the case of Ti–13Al, many twins seem to nucleate from a grain boundary but have not grown lengthwise to reach the opposite grain boundary, suggesting that any type of ordering has a significant impact on twin boundary migration as previously reported for Mg–Gd alloys [35]. Another factor for the dramatic decline of twinning activity might be found in the promotion of severe slip planarity in the presence of SRO and α_2. Figs. 8b and 11b demonstrate that ordering reduces the work hardening capability of the material, which has also been reported previously [4,28]. The absence of cross slip and dislocation interaction might reduce the ability of heterogeneous twin nucleation by twin dislocations. A suppression of cross slip makes dislocation jogs less common, which have been described as possible twin nuclei [55]. The jogs lower the energy for the separation of partial dislocations, and facilitate twin growth. In any case, ordering appears to be the reason why twinning is suppressed in Ti at high Al contents, either because it pins twin boundaries or because it promotes slip localization.

5. Conclusion

A systematic study of twin activity in Ti binary alloys with 0–13 at.% Al during uniaxial compression testing has been carried out in order to provide new insight into the effects of Al on twin activity in these alloys. Care was taken to obtain similar starting microstructures including textures to enable such comparison. One of the key microstructural features, ordering of Al in Ti, was characterised using large d-spacing neutron diffraction and selective diffraction aperture pattern imaging in the TEM. It is important to note that while Ti 10 at.% Al and Ti 13 at.% Al are known to form α_2 when aged in a certain temperature range and for long time, the heat treatments applied in the present study focused the work more on the effect of short range ordering. In order to monitor twin evolution in-situ loading experiments were carried out in combination with neutron diffraction in order to capture peak intensity changes, and the evolution of intergranular strains. In addition, detailed post mortem microstructure analysis by EBSD was carried out in order to identify twin types and quantify them. The main findings of the work can be summarised as follows:

- The neutron diffraction study on WISH revealed that Ti–Al binary alloys with up to 7 at.% Al showed practically no indication of SRO after annealing heat treatment followed by air cooling (100'sK/min). In contrast, Ti-10 at.% Al showed clear indication of short range ordering that became stronger with ageing or by further increasing Al content to 13 at.%. Aged Ti-7 at.% Al also showed a very slight indication of SRO. Long range ordering, i.e. α_2, was only identified for aged Ti 10 at.% Al and recrystallised Ti 13 at.% Al. In both cases only weak α_2 reflections were identified by TEM analysis and α_2 formed additionally to SRO.
- In the absence of ordering, alloys showed an increase in work hardenability with rising Al content, which can be correlated to a slight increase in $\{10\,\bar{1}2\}\langle 10\,\bar{1}1\rangle$ tensile twin activity confirmed by neutron diffraction and EBSD analysis. The increase in twin activity can be associated with ease of twin growth.
- In addition to the extremely dominant $\{10\,\bar{1}2\}\langle 10\,\bar{1}1\rangle$ tensile twinning mode, about 4% $\{11\,\bar{2}2\}\langle \bar{1}\bar{1}23\rangle$ compression twins were observed in Ti without any Al addition after a true strain of 0.09. In addition, EBSD analysis also revealed a small fraction of $\{11\,\bar{2}1\}\langle \bar{1}\bar{1}26\rangle$ tensile twins, which increases slightly with Al concentration, especially from to Ti–3Al to Ti–7Al.
- SRO significantly reduces the work hardenability of these alloys, which, apart from increased strain localisation, can be related to a dramatic reduction of twinning activity as identified during the in-situ loading experiments using neutron diffraction and post mortem EBSD analysis. Additional α_2 formation further emphasis this trend.
- It was found that with increasing Al content, in the absence of ordering, the critical residual intergranular strain required for twin nucleation decreases. This observation was interpreted as an indication that with increasing Al content in solution the intrinsic energy requirement for twin formation reduces, which could be due to an increase in stacking fault energy. However, the generally higher stress with increasing Al solute solution strengthening at which plasticity occurs might be the most important factor to increase twinning activity.
- The dramatic fall in twin activity in the presence of ordering, including short range ordering, is accompanied by a dramatic decrease in twin growth. It seems most likely that ordering dramatically reduces twin boundary mobility.

It should be noted that the initial increase in twinning activity with increasing Al content has not been shown previously as most studies have only focused on either commercially pure Ti or Ti with 6–7 wt.% Al. Considering the significant impact on work hardenability identified in the present study, Ti alloys with Al content not exceeding 7 at.% might be of particular importance when considering formability and sudden impact applications.

Acknowledgements

Allocation of the characterisation equipment in the Material Science Centre, Manchester and at ENGIN-X, ISIS is highly

appreciated, as well as discussions with staff from both facilities. The authors are grateful for funding from EPSRC (EP/H020047/1, EP/I005420/1, EP/I003290/1) and TIMET.

References

[1] J. Williams, R. Baggerly, N. Paton, Deformation behavior of HCP Ti-Al alloy single crystals, Metall. Mater. Trans. A 33 (2002) 837–850.
[2] G. Lutjering, J. Williams, Introduction, in: Titanium, second ed., Springer-Verlag Berlin and Heidelberg GmbH & Co, 2007.
[3] J. Jiang, A. Godfrey, W. Liu, Q. Liu, Microtexture evolution via deformation twinning and slip during compression of magnesium alloy AZ31, Mater. Sci. Eng. A 483–484 (2008) 576–579.
[4] D.J. Truax, C.J. McMahon Jr., Plastic behavior of titanium-aluminum alloys, Mater. Sci. Eng. 13 (1974) 125–139.
[5] M.J. Donachie, Titanium: a Technical Guide, ASM International, 2000.
[6] E.A. Metzbower, X-ray-line-profile analysis of titanium alloys, Metall. Trans. A 8 (1977) 279–282.
[7] E.A. Metzbower, Stacking fault probability determinations in HCP Ti–Al alloys, Metall. Mater. Trans. B 2 (1971) 3099–3103.
[8] T. Neeraj, M.J. Mills, Short-range order (SRO) and its effect on the primary creep behavior of a Ti–6wt.%Al alloy, Mater. Sci. Eng. A 319–321 (2001) 415–419.
[9] Z. Guo, A.P. Miodownik, N. Saunders, J.-P. Schillé, Influence of stacking-fault energy on high temperature creep of alpha titanium alloys, Scr. Mater. 54 (2006) 2175–2178.
[10] Y.B. Chun, S.H. Yu, S.L. Semiatin, S.K. Hwang, Effect of deformation twinning on microstructure and texture evolution during cold rolling of CP-titanium, Mater. Sci. Eng. A 398 (2005) 209–219.
[11] Y.B. Chun, M. Battaini, C.H.J. Davies, S.K. Hwang, Distribution characteristics of in-grain misorientation axes in cold-rolled commercially pure titanium and their correlation with active slip modes, Metall. Mater. Trans. A 41 (2010) 3473–3487.
[12] D.G.L. Prakash, R. Ding, R.J. Moat, I. Jones, P.J. Withers, J.Q.D. Fonseca, M. Preuss, Deformation twinning in Ti-6Al-4V during low strain rate deformation to moderate strains at room temperature, Mater. Sci. Eng. A 527 (2010) 5734–5744.
[13] S. Zaefferer, A study of active deformation systems in titanium alloys: dependence on alloy composition and correlation with deformation texture, Mater. Sci. Eng. A 344 (2003) 20–30.
[14] J.A. Venables, The electron microscopy of deformation twinning, J. Phys. Chem. Solids 25 (1964) 685–692.
[15] A. Rohatgi, K. Vecchio, G. Gray III, The influence of stacking fault energy on the mechanical behavior of Cu and Cu-Al alloys: deformation twinning, work hardening, and dynamic recovery, Metall. Mater. Trans. A 32 (2001) 135–145.
[16] Y. Zhang, N.R. Tao, K. Lu, Effect of stacking-fault energy on deformation twin thickness in Cu–Al alloys, Scr. Mater. 60 (2009) 211–213.
[17] J. Ghosh, S.K. Chattopadhayay, A.K. Meikap, S.K. Chatterjee, Microstructure characterization of titanium-base aluminium alloys by X-ray diffraction using Warren–Averbach and Rietveld method, J. Alloys Compd. 453 (2008) 131–137.
[18] J.W. Christian, S. Mahajan, Deformation twinning, Prog. Mater. Sci. 39 (1995) 1–157.
[19] H. Wood, G.D.W. Smith, A. Cerezo, Short range order and phase separation in Ti–Al alloys, Mater. Sci. Eng. A 250 (1998) 83–87.
[20] G. Lütjering, S. Weissmann, Mechanical properties of age-hardened titanium-aluminum alloys, Acta Metall. 18 (1970) 785–795.
[21] S. Sircar, K. Narasimhan, K. Mukherjee, An investigation of the ordered DO19 phase formation in the Ti-Al system, J. Mater. Sci. 21 (1986) 4143–4146.
[22] A.M. Chaze, C. Coddet, Influence of alloying elements on the dissolution of oxygen in the metallic phase during the oxidation of titanium alloys, J. Mater. Sci. 22 (1987) 1206–1214.
[23] J. Koike, K. Egashira, K. Maruyama, H. Oikawa, High temperature strength of α TiAl alloys with a locally ordered structure, Mater. Sci. Eng. A 213 (1996) 98–102.
[24] T.K.G. Namboodhiri, C.J. McMahon, H. Herman, Decomposition of the α-phase in titanium-rich Ti-Al alloys, Metall. Trans. 4 (1973) 1323–1331.
[25] T.K.G. Namboodhiri, On the Ti-Al phase diagram, Mater. Sci. Eng. 57 (1983) 21–22.
[26] A. Walle, M. Asta, First-principles investigation of perfect and diffuse antiphase boundaries in HCP-based Ti-Al alloys, Metall. Mater. Trans. A 33 (2002) 735–741.
[27] J. Williams, M. Blackburn, Strength, deformation modes and fracture in titanium-aluminium alloys, in: Trans. ASM, 1969, p. 398.
[28] T. Neeraj, D. Hou, G.S. Daehn, M.J. Mills, Phenomenological and microstructural analysis of room temperature creep in titanium alloys, Acta Mater. 48 (2000) 1225–1238.
[29] Y. Umakoshi, M. Yamaguchi, The stability and energies of planar faults in the DO19 ordered structure, Phys. Status Sol. (a) 68 (1981) 457–468.
[30] M. Thomas, A. Vassel, P. Veyssière, c slip in Ti3Al, Philos. Mag. A 59 (1989) 1013–1026.
[31] Y. Minonishi, Plastic deformation of single crystals of Ti3Al with D019 structure, Philos. Mag. A 63 (1991) 1085–1093.
[32] Y. Umakoshi, T. Nakano, T. Takenaka, K. Sumimoto, T. Yamane, Orientation and temperature dependence of yield stress and slip geometry of Ti3Al and Ti3Al-V single crystals, Acta Metall. Mater. 41 (1993) 1149–1154.
[33] M. Legros, A. Corn, D. Caillard, Prismatic and basal slip in Ti3Al I. Frictional forces on dislocations, Philos. Mag. A 73 (1996) 61–80.
[34] L.I. Yakovenkova, L.E. Kar'kina, Theoretical and experimental study of processes of deformation and fracture in single-crystal Ti3Al oriented for the basal slip, Phys. Metals Metallogr. 103 (2007) 531–554.
[35] F. Nie, M. Zhu, Z. Liu, Y. Fang, Periodic segregation of solute atoms in fully coherent twin boundaries, Science 340 (2013) 957–960.
[36] E.C. Oliver, M.R. Daymond, J. Quinta Da Fonseca, P.J. Withers, Intergranular stress evolution in titanium studied by neutron diffraction and self-consistent modelling, J. Neutron Res. 12 (2004) 33–37.
[37] J.L.W. Warwick, J. Coakley, S.L. Raghunathan, R.J. Talling, D. Dye, Effect of texture on load partitioning in Ti-6Al-4V, Acta Mater. 60 (2012) 4117–4127.
[38] J.L.W. Warwick, N.G. Jones, K.M. Rahman, D. Dye, Lattice strain evolution during tensile and compressive loading of CP Ti, Acta Mater. 60 (2012) 6720–6731.
[39] H. Abdolvand, M.R. Daymond, Internal strain and texture development during twinning: comparing neutron diffraction measurements with crystal plasticity finite-element approaches, Acta Mater. 60 (2012) 2240–2248.
[40] M. Lentz, M. Klaus, W. Reimers, B. Clausen, Effect of high temperature heat treatments on the deformation behavior of Mg–2%Mn–0.7%Ce extrusions investigated by in-situ energy-dispersive synchrotron X-ray diffraction and elasto-plastic self-consistent modeling, Mater. Sci. Eng. A 586 (2013) 178–189.
[41] M. Preuss, J.Q. da Fonseca, V. Allen, D.G.L. Prakash, M.R. Daymond, Twinning in structural material with a hexagonal close-packed crystal structure, J. Strain Anal. Eng. Des. 45 (2010) 377–390.
[42] J. Schuster, M. Palm, Reassessment of the binary Aluminum-Titanium phase diagram, J. Phase Equilib. Diffus. 27 (2006) 255–277.
[43] T.B. Massalski, H. Okamoto, P.R. Subramanian, L. Kacprzak, W.W. Scott Jr., M.A. Fleming, R. Boring, Binary Alloy Phase Diagrams, 1986.
[44] M.J. Philippe, C. Esling, B. Hocheid, Role of twinning in texture development and in plastic deformation of hexagonal materials, Texture Stress Microstruct. 7 (1988) 265–301.
[45] N. Bozzolo, L. Chan, A.D. Rollett, Misorientations induced by deformation twinning in titanium, J. Appl. Crystallogr. 43 (2010) 596–602.
[46] L.C. Chapon, P. Manuel, P.G. Radaelli, C. Benson, L. Perrott, S. Ansell, N.J. Rhodes, D. Raspino, D. Duxbury, E. Spill, J. Norris, Wish: the new powder and single crystal magnetic diffractometer on the second target station, Neutron News 22 (2011) 22–25.
[47] J.R. Santisteban, M.R. Daymond, J.A. James, L. Edwards, ENGIN-X: a third-generation neutron strain scanner, J. Appl. Crystallogr. 39 (2006) 812–825.
[48] M. Daymond, L. Edwards, Scientific review: ENGIN-X: a fully refined diffractometer designed specifically for measurement of stress, Neutron News 15 (2004) 24–29.
[49] C. Leyens, M. Peters, Titanium and Titanium Alloys, Wiley Online Library, 2003.
[50] G. Ghosh, A. van de Walle, M. Asta, First-principles calculations of the structural and thermodynamic properties of bcc, fcc and hcp solid solutions in the Al–TM (TM=Ti, Zr and Hf) systems: a comparison of cluster expansion and supercell methods, Acta Mater. 56 (2008) 3202–3221.
[51] F.H. Froes, C. Suryanarayana, D. Eliezer, Synthesis, properties and applications of titanium aluminides, J. Mater. Sci. 27 (1992) 5113–5140.
[52] M. Battaini, E.V. Pereloma, C.H.J. Davies, Orientation effect on mechanical properties of commercially pure titanium at room temperature, Metall. Mat. Trans. A 38 (2007) 276–285.
[53] G.J. Dienes, Lattice parameter and short-range order, Acta Metall. 6 (1958) 278–282.
[54] A.S. Shishmakov, R.A. Adamescu, D.A. Mirzayev, Stacking faults in alpha alloys of titanium, Phys. Metals Metallogr. 34 (1972) 219.
[55] J.A. Venables, Deformation twinning in face-centred cubic metals, Philos. Mag. 6 (1961) 379–396.